ARTICLES

Extensive Theoretical Study on Various Low-Lying Electronic States of Silicon Monochloride Cation Including Spin−Orbit Coupling

Kun Liu,[†] Le Yu,[†] and Wensheng Bian*

Beijing National Laboratory for Molecular Sciences, State Key Laboratory of Molecular Reaction Dynamics, Institute of Chemistry, Chinese Academy of Sciences, Beijing 100190, People's Republic of China

Received: October 30, 2008; Revised Manuscript Received: December 13, 2008

The potential energy curves of the 23 Ω states generated from the 12 valence Λ−S states of silicon monochloride cation are calculated for the first time using the internally contracted multireference configuration interaction method with the Davidson correction and entirely uncontracted cc-pV5Z basis set. Spin−orbit coupling is taken into account by the state interaction approach with the full Breit−Pauli Hamiltonian. Very good agreement is achieved between our computed spectroscopic properties and the available experimental data. In particular, the adiabatic excitation energies of the $a^3\Pi_{0+}$ and $a^3\Pi_1$ states computed by us are 31 708 and 31 830 cm^{-1}, respectively, in excellent agreement with the respective experimental values of 31 721 ± 2 and 31 836 ± 3 cm^{-1}. The curve crossings and the predissociation mechanism are investigated. The transition dipole moments are analyzed and the transition properties of the $a^3\Pi_{0+}-X^1\Sigma^+_{0+}$ and $a^3\Pi_1-X^1\Sigma^+_{0+}$ transitions are predicted, including the Franck−Condon factors and the radiative lifetimes.

1. Introduction

Chlorosilanes are used extensively in semiconductor industry,[1,2] and the fragment cations of chlorosilanes are found in the processes of plasma-enhanced chemical vapor deposition[3−6] and chlorine-based plasma etching,[7−9] in which silicon monochloride cation ($SiCl^+$) is a crucial reactive intermediate. For example, during the silicon-etching process in chlorine-based plasmas, $SiCl^+$ plays a significant role in the deposition of silicon on the reactor wall, and can be neutralized and returned into the plasma. There have been many experimental investigations on $SiCl^+$. In 1981, Tsuji et al.[10] reported the emission spectrum of $SiCl^+$ corresponding to the $a^3\Pi_{0+}-X^1\Sigma^+$ and $a^3\Pi_1-X^1\Sigma^+$ transitions by the flowing helium afterglow reaction of $SiCl_4$, and the spectroscopic constants of the $a^3\Pi_{0+}$, $a^3\Pi_1$, and $X^1\Sigma^+$ states were obtained by the vibrational analysis of the emission spectrum. Later, Weber and Armentrout[11] studied the reaction of Si^+ with $SiCl_4$ by the guided ion beam mass spectrometry and recommended the thermochemical values of $SiCl^+$ at 298 K. By the study of the reactions of O_2^+, Ar^+, and He^+ with $SiCl_4$, Fisher and Armentrout[12] derived some thermochemical values and the bond dissociation energy for $SiCl^+$. In 1993, the infrared diode laser spectrum for the ground state of $SiCl^+$ was measured in a hollow cathode discharge of $SiCl_4$ by Sumiyoshi et al.,[13] and the spectroscopic constants were also derived. In 1996, Reid[14] obtained the adiabatic excitation energy of the $a^3\Pi$ state of $SiCl^+$ and adiabatic electron affinity of SiCl by translational-energy spectroscopy. Subsequently, Marijnissen and ter Meulen[15] determined the value of adiabatic ionization potential (IP) of SiCl by mass-selected photoionization efficiency spectroscopy. More recently, many fundamental and hot band absorption lines of $SiCl^+$ were measured by Davies' group[16] with the help of diode laser velocity modulation spectroscopy, and a set of equilibrium parameters and spectroscopic constants for the $X^1\Sigma^+$ state was derived. Most of the above experimental studies were focused on the ground or the $a^3\Pi_{0+}$ and $a^3\Pi_1$ excited states, and little experimental information could be found for higher excited states of $SiCl^+$. In the chlorine-based plasmas, $SiCl^+$ may be present with different kinds of electronic excitation, and thus it would be very helpful to perform extensive theoretical studies on various low-lying electronic states of $SiCl^+$.

Several theoretical studies, mainly focused on the $X^1\Sigma^+$ ground state of $SiCl^+$, have been reported.[17−20] In addition, the $a^3\Pi$ and $A^1\Pi$ states have also been investigated by the ab initio configuration interaction method with a basis set at the double-ζ-plus-polarization level by Nishimura et al.[17] To the best of our knowledge, there has been no theoretical investigation on the other low-lying electronic states of $SiCl^+$. Furthermore, the spin−orbit (SO) coupling effects were not considered in all previous calculations. However, it is well-known that the SO coupling effects play an important role in spectroscopy and dynamics, even when the involved molecules are light. For example, the coupling of excited states of different spin multiplicities in the relevant region can lead to the spin−orbit-induced predissociation. The SO coupling effects may also make some regions of potential energy curves (PECs) very complex, especially when the avoided crossing rule is applied for the mixed Ω states.

In the present work, high-level ab initio calculations including the SO coupling effects have been performed to study various low-lying electronic states of $SiCl^+$. The PECs and spectroscopic constants of the 12 valence Λ−S states and 23 Ω states will be reported, various curve crossings, predissociation mechanisms, and SO coupling effects will be revealed, and the transition properties will also be predicted. The theoretical methods and computational details are briefly described in the next section, and in the third section we present our calculational results and the discussion. The conclusions are given in the last section.

* Corresponding author. Phone: (+86)10-62566307. E-mail: bian@iccas.ac.cn.
[†] Also at: Graduate University of the Chinese Academy of Sciences, Beijing 100049, People's Republic of China.

10.1021/jp809618y CCC: $40.75
Published on Web 02/09/2009

2. Methods and Computational Details

In this work, various basis sets have been tested, and finally the rather large entirely uncontracted Gaussian-type all-electron correlation consistent polarized valence quintuple zeta (cc-pV5Z) basis set[21] (20s12p4d3f2g1h) is chosen for both atoms in the calculation of Λ−S states. The active space that consists of eight electrons and eight molecular orbitals corresponding to 3s3p4s orbitals of Si and 3p orbitals of Cl is chosen for the complete active space self-consistent field (CASSCF) calculations, and this active space is referred to as CAS (8, 8). Additionally, the 3s electrons of Cl are put into the closed shell, and the rest of the electrons are kept frozen. The validity of CAS (8, 8) has been demonstrated in our previous study[22] on the silicon-containing diatomic cation SiF^+, in which various active spaces were carefully investigated, and CAS (8, 8) was shown to be a very good choice and to be able to give a nice description of the spectroscopic constants and potential energy curves of SiF^+.

The present calculations involve two $^1\Sigma^+$, one $^1\Sigma^-$, two $^1\Pi$, one $^1\Delta$, two $^3\Sigma^+$, one $^3\Sigma^-$, two $^3\Pi$, and one $^3\Delta$ states, where in the C_{2v} point group the Σ^+ state is obtained as A_1, Π as B_1 and B_2, Δ as A_1 and A_2, and Σ^- as A_2. Thus, a total of 18 electronic states of the C_{2v} symmetry, three A_1, two B_1, two B_2, and two A_2 for the singlet and triplet states, respectively, have been calculated using the MOLPRO 2002.6 program.[23] At a given internuclear distance of $SiCl^+$, the ground-state molecular orbitals are first calculated using the spin-restricted Hartree−Fock (HF) self-consistent field method, and then state-averaged CASSCF[24,25] calculations are carried out for the orbital optimization using the HF orbitals as the starting guess. Utilizing the CASSCF energies as reference values, the energies of each electronic state are computed by the internally contracted multireference configuration interaction method with the Davidson correction (icMRCI+Q).[26−28] This method has been successfully applied to the calculation of the excited states of other diatomic molecules, such as SCl[29] and SO^+.[30]

Scalar relativistic effects are taken into account through the second-order Douglas−Kroll[31] and Hess[32] one-electron integrals. The SO coupling effects are introduced into the calculations by the state interaction approach with the full Breit−Pauli Hamiltonian (H_{BP}),[33] which means that the SO eigenstates are obtained by diagonalizing $\hat{H}^{el} + \hat{H}^{so}$ in the basis of eigenfunctions of $\hat{H}^{el}$. In our SO coupling calculations, the $\hat{H}^{el}$ matrix elements are obtained from the icMRCI+Q calculations, while the $\hat{H}^{so}$ matrix elements are obtained from the CASSCF wave functions using the same basis set as mentioned before but removing the g and h functions. The PECs are plotted by connecting the calculated energy points with the aid of the avoided-crossing rule between the Ω electronic states of the same symmetry.

The nuclear Schrödinger equation is solved using Le Roy's LEVEL program[34] to obtain the spectroscopic constants, including the equilibrium bond length (R_e), the harmonic and anharmonic vibrational constants (ω_e and $\omega_e\chi_e$), the rotational constant (B_e), and the adiabatic relative electronic energy to the ground state (T_e). Dissociation energies (D_e) are obtained by comparing the molecular energies at the equilibrium internuclear distance and at a large separation for all electronic states, unless specified otherwise.

3. Results and Discussion

A. Basis Sets and Ionization Potentials. Using the methods described above, we calculate the spectroscopic constants of the ground-state $X^1\Sigma^+$ with various basis sets. These basis sets are obtained from the extensible computational chemistry environment basis set database.[35] Some of our calculational results together with previous experimental data are collected in Table 1 for comparison.

TABLE 1: Spectroscopic Constants of the $X^1\Sigma^+$ State of $SiCl^+$: Comparison of Different Basis Sets at the icMRCI+Q Level

basis sets[c]	R_e (Å)	ω_e (cm^{-1})	$\omega_e\chi_e$ (cm^{-1})	B_e (cm^{-1})	D_e (eV)
cc-pV5Z	1.9521	676.0	2.28	0.2846	5.265
cc-pV(5+d)Z	1.9519	676.3	2.28	0.2848	5.263
aug-cc-pV5Z	1.9524	675.1	2.28	0.2845	5.262
aug-cc-pV(5+d)Z	1.9520	675.7	2.28	0.2847	5.268
cc-pVQZ	1.9571	672.9	2.29	0.2832	5.176
cc-pV(Q+d)Z	1.9532	675.5	2.30	0.2843	5.214
aug-cc-pVQZ	1.9578	671.2	2.30	0.2830	5.188
expt.	1.9439[a]	678.2[a]	2.34[a]	0.2870[a]	5.29 ± 0.13[b]

[a] Reference 16. [b] Reference 12. [c] All of the basis sets used in the calculations are entirely uncontracted.

TABLE 2: Vertical and Adiabatic Ionization Potentials (IPs) for the $X^2\Pi$ State of SiCl

state of $SiCl^+$		vertical IP (eV)	adiabatic IP (eV)
$X^1\Sigma^+$ ($4\pi\rightarrow\infty$)	this work	7.32	7.18
	expt.	7.37[a]	7.33[b]
	other theory		7.16[c]
$a^3\Pi$ ($9\sigma\rightarrow\infty$)	this work	11.19	11.13
	expt.	11.24[a]	
$A^1\Pi$ ($9\sigma\rightarrow\infty$)	this work	12.59	
	other	12.15[d]	

[a] Reference 36. [b] Reference 15. [c] Obtained using the G2(MP2) method.[18] [d] The value suggested by Reid.[14]

As shown in Table 1, the spectroscopic constants computed with the uncontracted cc-pV5Z basis set are very similar to those obtained with uncontracted aug-cc-pV(5+d)Z and cc-pV(5+d)Z basis sets. Moreover, the convergence tendency from the quadruple zeta to the quintuple zeta basis sets is clearly shown in Table 1, and the spectroscopic constants obtained with the quintuple zeta basis sets are closer to the experimental values. The spectroscopic constants calculated with the uncontracted basis set of cc-pV5Z are in excellent agreement with the corresponding experimental values for the $X^1\Sigma^+$ state. For example, the R_e result differs from the experimental value[13] by only 0.0082 Å, and the ω_e, $\omega_e\chi_e$, and B_e results are only about 2.2, 0.06, and 0.0024 cm^{-1} smaller than the experimental values. The entirely uncontracted cc-pV5Z basis set is chosen for further calculations in this work in view of both the precision of the calculational results and the cost of the CPU time.

Our calculated vertical and adiabatic IPs for the $X^2\Pi$ state of SiCl along with the available literature values are listed in Table 2. We see that our vertical and adiabatic IPs to $X^1\Sigma^+$ $SiCl^+$ ($4\pi\rightarrow\infty$) are 7.32 and 7.18 eV, respectively, which are in good agreement with the experimental values of 7.37 eV[36] and 7.33 eV.[15] In addition, the adiabatic IP computed by Bauschlicher et al.[18] using the G2(MP2) method is 7.16 eV. Our computed vertical IPs of $X^2\Pi$ SiCl to the $a^3\Pi$ and $A^1\Pi$ states of $SiCl^+$ ($9\sigma\rightarrow\infty$) are 11.19 and 12.59 eV, respectively; the former is in excellent agreement with the experimental value of 11.24 eV,[36] whereas the latter is slightly larger than the value of 12.15 eV suggested by Reid.[14]

B. Potential Energy Curves and Spectroscopic Constants of the Λ−S States. Twelve Λ−S states of $SiCl^+$ are computed in this work, which correlate to the dissociation limit of the $Si^+(^2P, 3p^1)$ ion plus the $Cl(^2P, 3p^5)$ atom. The dominant configuration of the ground-state $X^1\Sigma^+$ is $1\sigma^2 2\sigma^2 3\sigma^2 4\sigma^2 1\pi^4 5\sigma^2 6\sigma^2 2\pi^4 7\sigma^2 8\sigma^2 3\pi^4 9\sigma^2 4\pi^0$. The $9\sigma\rightarrow 4\pi$ electronic excitation could generate the $^1\Pi$ and $^3\Pi$ states, whereas

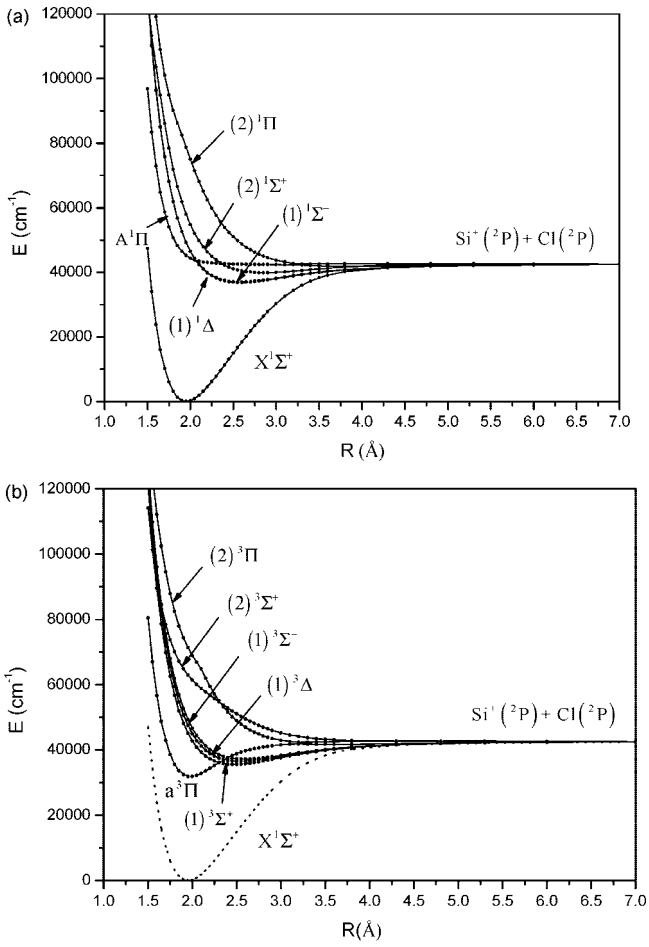

Figure 1. (a) Potential energy curves of the ground and low-lying singlet excited Λ−S states. (b) Potential energy curves of the ground and low-lying triplet excited Λ−S states.

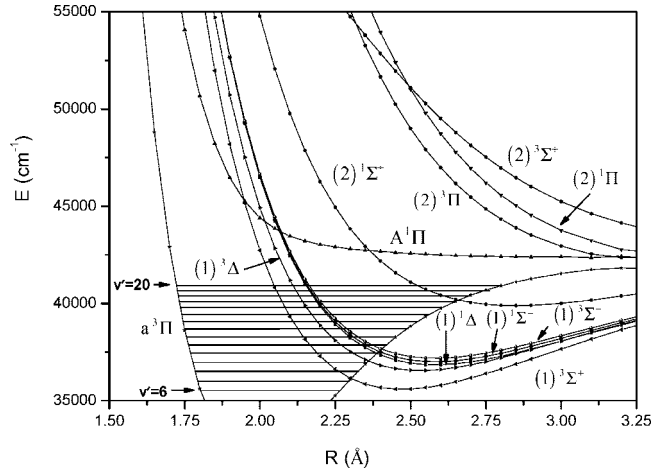

Figure 2. An amplified view of the crossing region of the potential energy curves together with the vibrational levels of the $a^3\Pi$ state.

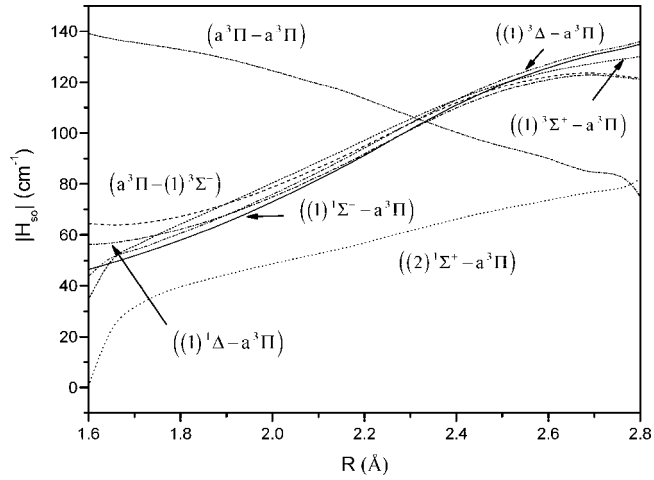

Figure 3. Evolution of the absolute values of spin−orbit matrix elements related to the $a^3\Pi$ state with the internuclear distance in the curve crossing region. (See Table 4 for the definition of these spin−orbit matrix elements.)

the $3\sigma \rightarrow 4\sigma$ excitation could generate the $^1\Sigma^+$, $^1\Sigma^-$, $^1\Delta$, $^3\Sigma^+$, $^3\Sigma^-$, and $^3\Delta$ states. In Figure 1, the PECs of the ground and low-lying excited states computed with the icMRCI+Q method are plotted, and it can be seen that there are eight bound states in total. The computed spectroscopic constants for bound states are listed in Table 3. As shown in Figure 1 and Table 3, only the ground state and the lowest excited state, $a^3\Pi$ state, have potential wells deeper than 1 eV. Our computed spectroscopic constants of the ground state reproduce the experimental data well, and the agreement is better than that achieved by Nishimura et al.[17] As for the $a^3\Pi$ state, our calculated T_e value of 31 832 cm^{-1} is in very good agreement with the value of 31 836 ± 3 cm^{-1} derived from experiment[10] for the $a^3\Pi_1$ state, although the SO splitting will be discussed in section 3D. In addition, our calculated T_e value is consistent with the experimental value of 31 778 ± 1613 cm^{-1}.[14] Table 3 also shows that there are six other bound excited Λ−S states [$(1)^3\Sigma^+$, $(1)^3\Delta$, $(1)^1\Delta$, $(1)^1\Sigma^-$, $(1)^3\Sigma^-$, $(2)^1\Sigma^+$], which have not been reported before, distributed in the region from 35 000 to 40 000 cm^{-1}. These states cross, mix, and strongly interact with one another. These bound low-lying Λ−S states (except for $(2)^1\Sigma^+$) have relatively deep wells, with the depths for the $(1)^3\Sigma^+$, $(1)^3\Delta$, $(1)^1\Delta$, $(1)^1\Sigma^-$, and $(1)^3\Sigma^-$ states being 0.876, 0.757, 0.720, 0.700, and 0.697 eV, respectively. All of these are deeper than those for SiF^+, as a result of which these states cross with the $a^3\Pi$ state at much lower vibrational levels than in the case of SiF^+.[22] The crossings between the $a^3\Pi$ and $(1)^3\Sigma^+$, $(1)^3\Delta$, $(1)^1\Delta$, $(1)^1\Sigma^-$, $(1)^3\Sigma^-$, and $(2)^1\Sigma^+$ states will lead to the predissociation of the $a^3\Pi$ state, which will be discussed in detail in the next section. Besides the $a^3\Pi$ state, the $A^1\Pi$ state also crosses with the six bound states at higher energies. For the $A^1\Pi$ state, we do not find any potential well and its PEC is repulsive, as is consistent with the previous theoretical[17] results and the experimental observation[10] that the $A^1\Pi - X^1\Sigma^+$ emission could not be found. The bound excited $(2)^1\Sigma^+$ state, whose equilibrium bond length of 2.8485 Å is almost 1 Å larger than that of the ground state, is repulsive in the Franck−Condon region and has a flat potential well at large internuclear distances. So the Franck−Condon factors for the $(2)^1\Sigma^+$ state should be small, and the transition from the ground state to the $(2)^1\Sigma^+$ state would be hard to observe in experiment. Except for the $a^3\Pi$ and $(2)^1\Sigma^+$ states, the other bound excited states are shown to have equilibrium bond lengths, which are about 0.5−0.65 Å larger than that of the ground state. Furthermore, the PECs for the $(2)^3\Sigma^+$, $(2)^1\Pi$, and $(2)^3\Pi$ states are also repulsive without any type of minimum in the whole range.

C. Curve Crossing and Predissociation. As mentioned above, the $a^3\Pi$ state crosses with the $(1)^3\Sigma^+$, $(1)^3\Delta$, $(1)^1\Delta$, $(1)^1\Sigma^-$, $(1)^3\Sigma^-$, and $(2)^1\Sigma^+$ states. An amplified view of the

TABLE 3: Theoretical Spectroscopic Constants of the Low-Lying Λ−S States of $SiCl^+$

Λ−S state	T_e (cm^{-1})	R_e (Å)	ω_e (cm^{-1})	$\omega_e\chi_e$ (cm^{-1})	B_e (cm^{-1})	D_e (eV)
$X^1\Sigma^+$	0	1.9521	676.0	2.28	0.2846	5.265
expt.		1.9439[a]	678.2[a]	2.34[a]	0.2870 [a]	5.29 ± 0.13[b]
expt.[c]		1.9439	678.3	2.36	0.2870	
other theory		1.971[d]	673[d]	2.9[d]	0.279[d]	5.239[e]
$A^3\Pi$	31 832	1.9806	601.4	7.01	0.2765	1.332
expt.[f]	31 778 ± 1613					
expt.[g] ($a^3\Pi_1$)	31 836 ± 3		596.0 ± 1.8	6.75 ± 0.56		
other theory[d]	30 900	2.020	524	8.6	0.266	
$(1)^3\Sigma^+$	35 523	2.4711	257.1	2.29	0.1776	0.876
$(1)^3\Delta$	36 487	2.5308	237.6	2.29	0.1693	0.757
$(1)^1\Delta$	36 785	2.5792	229.1	2.25	0.1631	0.720
$(1)^1\Sigma^-$	36 946	2.5792	226.9	2.27	0.1631	0.700
$(1)^3\Sigma^-$	37 122	2.5805	224.3	2.31	0.1629	0.679
$(2)^1\Sigma^+$	39 828	2.8485	163.7	1.87	0.1337	0.345

[a] Reference 16. [b] Reference 12. [c] Reference 13. [d] Reference 17. [e] The D_0 value obtained with the G2(MP2) method.[18] [f] Reference 14. [g] Reference 10.

TABLE 4: Spin−Orbit Matrix Elements between Two Interacting Electronic States in the Curve Crossing Region[a]

spin−orbit matrix elements
$i\langle a^3\Pi_x, m_s = 1 \lvert L_zS_z\rvert a^3\Pi_y, m_s = 1\rangle = (a^3\Pi - a^3\Pi)$
$\langle (1)^3\Sigma^+, m_s = 0 \lvert L_yS_y\rvert a^3\Pi_x, m_s = 1\rangle = ((1)^3\Sigma^+ - a^3\Pi)$
$\langle (1)^3\Delta_x, m_s = 0 \lvert L_yS_y\rvert a^3\Pi_x, m_s = 1\rangle = ((1)^3\Delta - a^3\Pi)$
$\langle (1)^1\Delta_x, m_s = 0 \lvert L_yS_y\rvert a^3\Pi_x, m_s = 1\rangle = ((1)^1\Delta - a^3\Pi)$
$i\langle (1)^1\Sigma^-, m_s = 0 \lvert L_xS_x\rvert a^3\Pi_x, m_s = 1\rangle = ((1)^1\Sigma^- - a^3\Pi)$
$i\langle a^3\Pi_x, m_s = 0 \lvert L_xS_x\rvert (1)^3\Sigma^-, m_s = 1\rangle = (a^3\Pi - (1)^3\Sigma^-)$
$\langle (2)^1\Sigma^+, m_s = 0 \lvert L_yS_y\rvert a^3\Pi_x, m_s = 1\rangle = ((2)^1\Sigma^+ - a^3\Pi)$

[a] In parentheses is given the schematic representation used in Figure 3.

TABLE 5: Dissociation Relationships of the Low-Lying Ω States of $SiCl^+$

		energy (cm^{-1})	
atomic state (Si^++Cl)	Ω state	theory	expt.[a]
$^2P_{1/2}+^2P_{3/2}$	$2,1,1,0^+,0^-$	0	0
$^2P_{3/2}+^2P_{3/2}$	$3,2,2,1,1,1,0^+,0^+,0^-,0^-$	263	287
$^2P_{1/2}+^2P_{1/2}$	$1,0^+,0^-$	836	881
$^2P_{3/2}+^2P_{1/2}$	$2,1,1,0^+,0^-$	1099	1168

[a] Reference 38.

crossing region is given in Figure 2, which covers the energy range of 35 000−55 000 cm^{-1}. Besides the crossings between the $a^3\Pi$ state and several other states, we can also notice from Figure 2 that the $A^1\Pi$ state crosses with the $(1)^3\Sigma^+$, $(1)^3\Delta$, $(1)^1\Delta$, $(1)^1\Sigma^-$, and $(1)^3\Sigma^-$ states at $R \simeq 1.95-2.07$ Å, and with the $(2)^1\Sigma^+$ state at $R = 2.36$ Å, and the $(2)^3\Sigma^+$ state crosses with the $(2)^1\Pi$ and $(2)^3\Pi$ states at larger R values. As shown in Figure 2, the $\nu' < 7$ vibrational levels of the $a^3\Pi$ state are expected to have long lifetimes because of being free from any interaction with other states, while the upper levels ($\nu' \geq 7$), which are located at or above the crossings of the $a^3\Pi$ state with other states, may be predissociated. So the predissociation of the $a^3\Pi$ state for $SiCl^+$ appears at much lower vibrational levels than that for SiF^+, for which the $a^3\Pi$ state crosses with other states at much higher energy levels ($\nu' > 18$) as revealed in our previous work.[22] Other evident differences for the crossing pattern between $SiCl^+$ and SiF^+ could also be noticed; for example, in our previous work on SiF^+,[22] an avoided crossing between $(1)^3\Sigma^+$ and $(2)^3\Sigma^+$ was found, whereas the $(2)^3\Sigma^+$ state is far away from the $(1)^3\Sigma^+$ state in the case of $SiCl^+$ (see Figure 2).

The predissociation mechanisms could be studied in a quantitative way by using the wave packet method with the predissociation lifetimes being computed.[37] Considering the main purpose of our work, in the following we present a qualitative analysis on the predissociation of the $a^3\Pi$ state with the help of the computed SO matrix elements. The absolute values of SO matrix elements as functions of internuclear distances in the curve crossing region are depicted in Figure 3, and the definitions of the schematic representation for the SO matrix elements used in the figure are given in Table 4. We can see from the figure that the SO matrix elements involving two interacting electronic states increase monotonously when the internuclear distance increases from 1.6 to 2.8 Å, with the exception of the $(a^3\Pi - a^3\Pi)$ state, which decreases with the increase of the internuclear distance. The $a^3\Pi$ state crosses with several states at a wide range of vibrational levels, and the following predissociation pathways are possible: $a^3\Pi(\nu' \geq 7) \rightarrow (1)^3\Sigma^+$, $a^3\Pi(\nu' \geq 9) \rightarrow (1)^3\Delta$, $a^3\Pi(\nu' \geq 10) \rightarrow (1)^1\Delta$, $a^3\Pi(\nu' \geq 10) \rightarrow (1)^1\Sigma^-$, $a^3\Pi(\nu' \geq 10) \rightarrow (1)^3\Sigma^-$, and $a^3\Pi(\nu' \geq 17) \rightarrow (2)^1\Sigma^+$ (see Figure 2). The predissociation pathways of $a^3\Pi \rightarrow (1)^1\Delta$, $a^3\Pi \rightarrow (1)^1\Sigma^-$, and $a^3\Pi \rightarrow (2)^1\Sigma^+$ involve states of different spin multiplicities, and further investigations are required to see whether this kind of predissociation could be induced by the SO coupling. As shown in Figure 3, the absolute values of our computed SO matrix elements of the interacting electronic states in the curve crossing region of 2.3−2.7 Å are all larger than 60 cm^{-1}, which is enough to induce this kind of triplet−singlet predissociation mentioned above. From Figure 3, we could also notice that the SO matrix elements between the $a^3\Pi$ and $(2)^1\Sigma^+$ electronic states are evidently lower than others; in addition, the predissociation pathway of $a^3\Pi \rightarrow (2)^1\Sigma^+$ occurs at much higher vibrational levels ($\nu' \geq 17$) than others. So the influence of the $a^3\Pi \rightarrow (2)^1\Sigma^+$ pathway would be very small. Summing up, the predissociation of the $SiCl^+$ $a^3\Pi$ electronic state starts around the $\nu' = 7$ vibrational level via the $(1)^3\Sigma^+$ state; for $a^3\Pi$ $\nu' \geq 9$ levels, a few closely mixed predissociation channels involving the $(1)^3\Delta$, $(1)^1\Delta$, $(1)^1\Sigma^-$, and $(1)^3\Sigma^-$ states would be open; it is expected that the $\nu' = 10$ level would predissociate rapidly.

D. Potential Energy Curves and Spectroscopic Constants of the Ω States. The dissociation limit $Si^+(^2P)+Cl(^2P)$ splits into four asymptotes when the SO coupling is taken into account, $Si^+(^2P_{1/2})+Cl(^2P_{3/2})$, $Si^+(^2P_{3/2})+Cl(^2P_{3/2})$, $Si^+(^2P_{1/2})+Cl(^2P_{1/2})$, and $Si^+(^2P_{3/2})+Cl(^2P_{1/2})$. The calculated energy separations are 263 cm^{-1} ($^2P_{1/2}-^2P_{3/2}$ of Si^+) and 836 cm^{-1} ($^2P_{3/2}-^2P_{1/2}$ of Cl),

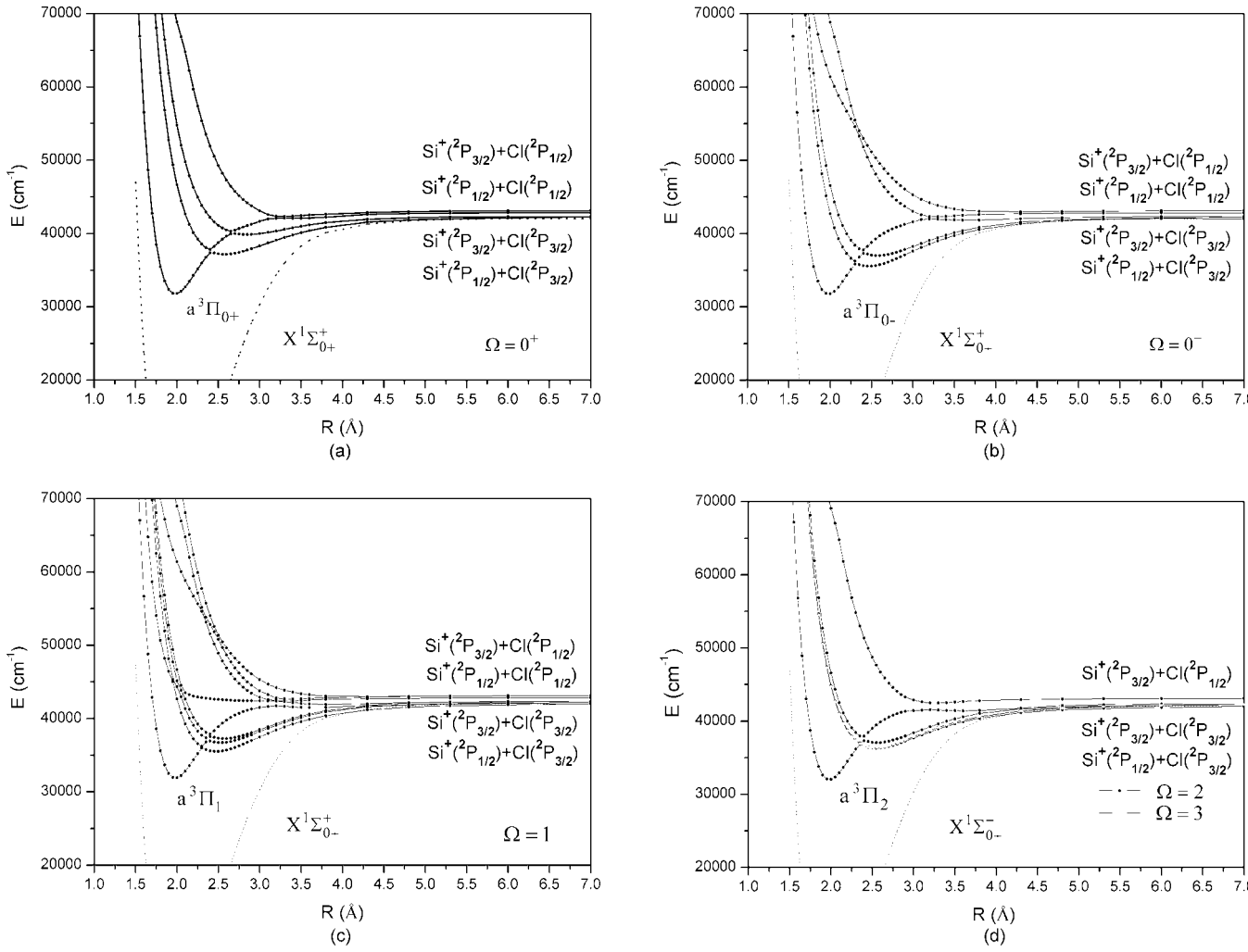

Figure 4. Potential energy curves of $SiCl^+$ for (a) $\Omega = 0^+$, (b) $\Omega = 0^-$, (c) $\Omega = 1$, (d) $\Omega = 2$ and 3 states, respectively. The dotted line in (b), (c), and (d) is the curve of the ground $X0^+$ state.

which are in good agreement with the observed values of 287 and 881 cm^{-1},[38] respectively. The dissociation relationships for the possible Ω states and corresponding energy separations are given in Table 5. Altogether, there are 23 Ω states of 0^+, 0^-, 1, 2, and 3 symmetries, which split into four asymptotes within only 1099 cm^{-1}.

The computed PECs for the five states of $\Omega = 0^+$, five states of $\Omega = 0^-$, eight states of $\Omega = 1$, four states of $\Omega = 2$, and one state of $\Omega = 3$ are plotted separately in Figure 4a−d. The spectroscopic constants and dominant Λ−S state compositions at R_e of the bound states obtained by solving the nuclear Schrödinger equations are given in Table 6. The ground-state $X0^+$, which is composed of 100% $X^1\Sigma^+$ at R_e, has almost the same spectroscopic properties as the pure Λ−S ground-state $X^1\Sigma^+$, except that its calculational D_e value of 5.212 eV is 0.053 eV smaller than that for $X^1\Sigma^+$.

For the $a^3\Pi$ state, the PECs for the four Ω components, 0^-, 0^+, 1, and 2, have well depths of 1.292, 1.324, 1.276, and 1.260 eV, respectively. Their energies increase in the order of 0^-, 0^+, 1, and 2 near the equilibrium bond lengths, and the largest splitting among the components of the $a^3\Pi$ state ($(1)0^- - (1)2$) is computed to be 252 cm^{-1}. Two components of the $a^3\Pi$ state (0^+ and 1) have been observed in experiment,[10] and excellent agreement is acquired between the values obtained from the vibrational analysis of the emission spectrum[10] and our calculated results. For the $a^3\Pi_{0+}$ state, our computed ω_e and $\omega_e\chi_e$ values of 598.4 and 6.55 cm^{-1} are in very good agreement with the experimental values of 595.8 ± 1.0 and 6.62 ± 0.12 cm^{-1}; and for the $a^3\Pi_1$ state, our computational ω_e and $\omega_e\chi_e$ values of 598.9 and 6.71 cm^{-1} are also very close to the experimental values of 596.0 ± 1.8 and 6.75 ± 0.56 cm^{-1}.[10] The adiabatic excitation energies of the $a^3\Pi_{0+}$ and $a^3\Pi_1$ states obtained by us are 31 708 and 31 830 cm^{-1}, respectively, which are in excellent agreement with the experimental values of 31 721 ± 2 and 31 836 ± 3 cm^{-1},[10] and the corresponding energy splitting of 122 cm^{-1} also closely matches the experimental value of 115 cm^{-1}.[10]

The $a^3\Pi$ state crosses with the closely spaced $(1)^3\Sigma^+$, $(1)^3\Delta$, $(1)^1\Delta$, $(1)^1\Sigma^-$, $(1)^3\Sigma^-$ states and the $(2)^1\Sigma^+$ state in the internuclear distance region of 2.3−2.7 Å, and when the SO coupling effects are introduced, the shape and character of the PECs would change distinctly, because these crossings are near the well bottoms of the six states. Because of this point, and the avoided crossing rule between different Ω states, the shapes of the PECs for the Ω states will differ from the pure Λ−S states evidently, and the PECs of the Ω states with potential wells would become unsmooth. For example, we can see in Figure 4a−d that some Ω states have two minima on their PECs. This would make the calculation of the spectroscopic constants of these states somewhat more difficult.

E. Transition Properties. The Einstein coefficient for spontaneous emission ($A_{v',v''}$), which is equivalent to the rate that the molecules radiate from the excited state to the ground

TABLE 6: Spectroscopic Constants of the Bound Low-Lying Ω States of $SiCl^+$

Ω states	T_e (cm^{-1})	R_e (Å)	ω_e (cm^{-1})	$\omega_e\chi_e$ (cm^{-1})	B_e (cm^{-1})	D_e (eV)	dominant Λ−S composition at R_e (%)
$X0^+$	0	1.9521	676.1	2.28	0.2846	5.212	100.0 $X^1\Sigma^+$
expt.[a]		1.9439	678.2	2.34	0.2870		
expt.[b]		1.9439	678.3	2.36	0.2870		
expt.			679.1 ± 2.0[c]	2.43 ± 0.52[c]		5.29 ± 0.13[d]	
$(1)0^-$	31 705	1.9804	598.5	6.40	0.2765	1.292	100.0 $a^3\Pi$
$(2)0^+$	31 708	1.9803	598.4	6.55	0.2765	1.324	100.0 $a^3\Pi$
expt.[c]	31 721 ± 2		595.8 ± 1.0	6.62 ± 0.12			
(1)1	31 830	1.9807	598.9	6.71	0.2764	1.276	100.0 $a^3\Pi$
expt.[c]	31 836 ± 3		596.0 ± 1.8	6.75 ± 0.56			
(1)2	31 957	1.9810	597.8	6.59	0.2764	1.260	100.0 $a^3\Pi$
(2)1	36 129	2.2941	206.2	0.55	0.2227	0.745	57.3 $(1)^3\Sigma^+$, 39.3 $a^3\Pi$, 2.5 $(1)^3\Sigma^-$
$(2)0^-$	36 203	2.2966	356.8	13.91	0.2268	0.768	69.8 $(1)^3\Sigma^+$, 28.6 $a^3\Pi$, 1.6 $(1)^1\Sigma^-$
(1)3	36 295	2.5311	237.6	2.29	0.1693	0.757	100.0 $(1)^3\Delta$
(2)2	36 597	2.3474	163.0	4.23	0.1667	0.671	68.8 $(1)^1\Delta$, 28.9 $(1)^3\Delta$, 2.3 $a^3\Pi$
(3)1	37 185	2.5730	191.8	0.47	0.1610	0.647	93.9 $(1)^3\Sigma^-$, 5.3 $(1)^3\Sigma^+$
$(3)0^-$	37 686	2.3891	595.8	22.15	0.1907	0.585	51.4 $a^3\Pi$, 46.7 $(1)^1\Sigma^-$, 1.9 $(1)^3\Sigma^+$
$(3)0^+$	37 762	2.3988	532.4	26.03	0.1898	0.577	66.6 $(1)^3\Sigma^-$, 33.2 $a^3\Pi$
(4)1	37 817	2.3930	617.4	25.73	0.1900	0.569	52.3 $(1)^3\Sigma^-$, 41.7 $a^3\Pi$, 3.1 $(1)^3\Delta$, 2.7 $(1)^3\Sigma^+$
(3)2	37 823	2.3792	621.6	26.21	0.1923	0.563	62.5 $(1)^1\Delta$, 18.9 $a^3\Pi$, 18.5 $(1)^3\Delta$
$(4)0^+$	40 250	2.6500	364.0	16.91	0.1548	0.340	69.6 $(2)^1\Sigma^+$, 29.7 $a^3\Pi$
(5)1	41 867	3.8311	62.7	2.59	0.0739	0.069	58.7 $A^1\Pi$, 26.5 $a^3\Pi$, 12.3 $(2)^3\Sigma^+$
$(4)0^-$	42 249	3.2660	110.7	5.80	0.1020	0.093	95.0 $(2)^3\Pi$, 4.0 $a^3\Pi$
$(5)0^+$	42 271	3.2709	119.6	5.05	0.1014	0.123	90.6 $(2)^3\Pi$, 8.0 $a^3\Pi$
(6)1	42 320	3.3117	96.1	5.13	0.0993	0.085	57.9 $(2)^3\Pi$, 31.3 $A^1\Pi$, 6.1 $(2)^1\Pi$, 3.34 $a^3\Pi$
(4)2	42 399	3.2450	119.8	5.81	0.1032	0.107	97.8 $(2)^3\Pi$
(7)1	42 615	3.3640	81.9	3.97	0.0959	0.080	89.0 $(2)^1\Pi$, 9.0 $(2)^3\Pi$

[a] Reference 16. [b] Reference 13. [c] Reference 10. [d] Reference 12.

TABLE 7: Franck−Condon Factors of the $a^3\Pi_{0+}-X^1\Sigma^+_{0+}$ and $a^3\Pi_1-X^1\Sigma^+_{0+}$ Transitions

	$\nu''=0$	$\nu''=1$	$\nu''=2$	$\nu''=3$	$\nu''=4$	$\nu''=5$	$\nu''=6$	$\nu''=7$
$a^3\Pi_{0+}-X^1\Sigma^+_{0+}$								
$\nu'=0$	0.8783	0.1109	0.0100	0.0007	0.0000	0.0000	0.0000	0.0000
$\nu'=1$	0.1152	0.6463	0.2039	0.0310	0.0033	0.0003	0.0000	0.0000
$\nu'=2$	0.0063	0.2198	0.4297	0.2701	0.0631	0.0096	0.0012	0.0001
$\nu'=3$	0.0002	0.0220	0.3023	0.2409	0.3020	0.1056	0.0225	0.0038
$\nu'=4$	0.0000	0.0010	0.0502	0.3525	0.0953	0.2897	0.1534	0.0454
$A^3\Pi_1-X^1\Sigma^+_{0+}$								
$\nu'=0$	0.8754	0.1133	0.0105	0.0008	0.0000	0.0000	0.0000	0.0000
$\nu'=1$	0.1178	0.6387	0.2074	0.0322	0.0035	0.0003	0.0000	0.0000
$\nu'=2$	0.0067	0.2237	0.4194	0.2732	0.0654	0.0102	0.0013	0.0002
$\nu'=3$	0.0002	0.0231	0.3059	0.2301	0.3030	0.1091	0.0238	0.0041
$\nu'=4$	0.0000	0.0011	0.0525	0.3540	0.0866	0.2870	0.1573	0.0479

state, determines the radiative lifetime. The radiative lifetime for a given vibrational level ν' can be calculated by the following formula:[39,40]

$$\tau_{v'} = 1/\left[\sum_{v'';J';J''}\left(\frac{(J'+J''+1)e^{-hcB_{v'}J'(J'+1)/\kappa T}}{\sum_{J',J''}(J'+J''+1)e^{-hcB_{v'}J'(J'+1)/\kappa T}}A_{v',v'';J',J''}\right)\right]$$
$$= 1/\left[\sum_{v''}A_{v',v''}\right] = \frac{3h}{64\pi^4\cdot(\sum_{v''}q_{v',v''}\Delta E^3_{v',v''})\cdot|a_0\cdot e\cdot \mathrm{TDM}|^2}$$
$$= \frac{4.9355\times10^5}{(\sum_{v''}q_{v',v''}\Delta E^3_{v',v''})\cdot|\mathrm{TDM}|^2} \quad (1)$$

In the above equation, $q_{v',v''}$ is the Franck−Condon factor, TDM is the averaged transition dipole moment in the atomic units, the energy difference $\Delta E_{v',v''}$ is in cm^{-1}, and $\tau_{v'}$ is in seconds.

The intensity distribution in a band system can largely be explained by the Franck−Condon principle. The Franck−Condon factors of the $a^3\Pi_{0+}-X^1\Sigma^+_{0+}$ and $a^3\Pi_1-X^1\Sigma^+_{0+}$ transitions are evaluated by the LEVEL program and listed in Table 7. It is obvious that the ($\nu'=0\rightarrow\nu''=0$) transitions have the maximum Franck−Condon factors, and as the values of ν' and ν'' increase, the Franck−Condon factors of $\Delta\nu=0$ bands decrease rapidly, and these are qualitatively consistent with the emission spectra experiment of Tsuji et al.[10]

The transition dipole moments (TDMs) of the allowed transitions between the bound excited Ω states and the ground state as functions of the bond distance are plotted in Figure 5, which are computed at the CASSCF level of theory. The transition of $(4)0^+-X0^+$ has larger TDMs at internuclear distances smaller than 2.65 Å, while the transition of $(3)0^+-X0^+$ has larger TDMs at internuclear distances larger than 2.65 Å. As the $A^1\Pi-X^1\Sigma^+$ and $(2)^1\Sigma^+-X^1\Sigma^+$ transitions belong to the singlet−singlet allowed transitions, the TDMs of them are much larger than those of the triplet−singlet forbidden transitions. The transitions from the Ω states, which are mainly composed of the $(2)^1\Sigma^+$ or $A^1\Pi$ state to the ground $X0^+$ state, have much larger TDMs than do the other transitions. At the internuclear distance smaller than 2.65 Å, the $(4)0^+$ state is mainly composed of the $(2)^1\Sigma^+$ state, while at the internuclear distance larger than

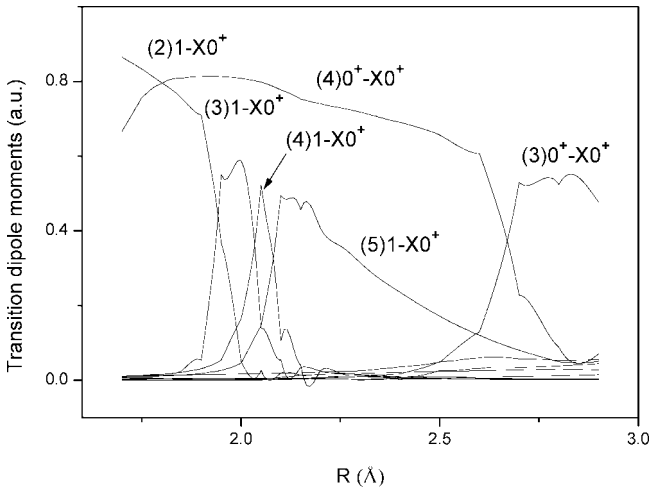

Figure 5. Transition dipole moments between the bound excited Ω states and the ground state of $SiCl^+$.

TABLE 8: Radiative Lifetimes (in ms) of the Transitions from the $a^3\Pi_{0+}$ and $a^3\Pi_1$ Low Vibrational Levels to the $X^1\Sigma^+_{0+}$ State

	radiative lifetimes				
transitions	$\nu' = 0$	$\nu' = 1$	$\nu' = 2$	$\nu' = 3$	$\nu' = 4$
$a^3\Pi_{0+}-X^1\Sigma^+_{0+}$	6.20	3.58	2.53	1.86	1.37
$a^3\Pi_1-X^1\Sigma^+_{0+}$	0.483	0.490	0.496	0.504	0.517

2.65 Å, the $(3)0^+$ state is mainly composed of the $(2)^1\Sigma^+$ state, and this could be the reason why they have larger TDMs at the corresponding internuclear distances. We can also see from Figure 5 that the TDMs of (3)1, (4)1, and (5)1 states to the $X0^+$ state have maximum values at the internuclear distances of 1.98, 2.05, and 2.11 Å, respectively. Similarly, these could be explained by the fact that the (3)1, (4)1, and (5)1 states are all dominantly composed of the $A^1\Pi$ state at the respective maximum points.

The radiative lifetimes of the transitions from the $a^3\Pi_{0+}$ and $a^3\Pi_1$ low vibrational levels to the ground state are computed and listed in Table 8. We can see that the radiative lifetimes of the $a^3\Pi_{0+}-X^1\Sigma^+_{0+}$ and $a^3\Pi_1-X^1\Sigma^+_{0+}$ transitions are both of the order of milliseconds, and the lifetimes of the $a^3\Pi_{0+}-X^1\Sigma^+_{0+}$ transition are longer (ranging from 3 to 13 times) than those of the $a^3\Pi_1-X^1\Sigma^+_{0+}$ transition. The energy separations, TDMs, and the Franck−Condon factors would affect the radiative lifetimes, and the above two transitions have similar energy separations and Franck−Condon factors. Consequently, according to the calculational formula of the radiative lifetime shown above, the relatively short lifetimes of the $a^3\Pi_1-X^1\Sigma^+_{0+}$ transition are because of its larger TDMs.

4. Conclusions

All 23 Ω states generated from the 12 Λ−S states of $SiCl^+$ have been computed for the first time. The icMRCI+Q methods with the Douglas−Kroll scalar relativistic correction and the entirely uncontracted all-electron cc-pV5Z basis set are used, and the SO coupling matrix elements are computed using the state interaction approach with the full Breit−Pauli Hamiltonian. The PECs of all valence states are obtained, and six bound excited Λ−S states $[(1)^3\Sigma^+, (1)^3\Delta, (1)^1\Delta, (1)^1\Sigma^-, (1)^3\Sigma^-, (2)^1\Sigma^+]$ are revealed for the first time. The spectroscopic constants of bound states are calculated, and our results reproduce the available experimental values very well. The errors of the theoretical R_e, ω_e, $\omega_e\chi_e$, and B_e results for the ground state are only 0.0082 Å, 2.2 cm^{-1}, 0.06 cm^{-1}, and 0.0024 cm^{-1}, respectively. The adiabatic excitation energies of the $a^3\Pi_{0+}$ and $a^3\Pi_1$ states computed by us are 31 708 and 31 830 cm^{-1}, respectively, in excellent agreement with the respective experimental values of 31 721 ± 2 and 31 836 ± 3 cm^{-1}. The calculated ionization potentials of the ground-state SiCl to a few states of $SiCl^+$ are in good agreement with the experimental results.

Our calculations also show that the $a^3\Pi$ state crosses with several other states, and the SO coupling has obvious effects on the PEC shape, and the excitation and dissociation energies. With the help of the calculated SO coupling matrix elements, the predissociation mechanisms of the $a^3\Pi$ state are analyzed. It is found that the predissociation of the $a^3\Pi$ state for $SiCl^+$ appears at much lower vibrational levels than that for SiF^+, and we predict that the spectra of the $\nu' \geq 7$ band of the $a^3\Pi$ $SiCl^+$ may become diffused. Our calculations indicate that the consideration of the SO coupling effects is absolutely necessary for the study of $SiCl^+$. Our calculations on the transition properties show that the TDMs of the $(4)0^+-X0^+$ transition are larger than those of the other transitions at a majority of internuclear distances considered, and the radiative lifetimes of the $a^3\Pi_{0+}-X^1\Sigma^+_{0+}$ transition are 3−13 times longer than those of the $a^3\Pi_1-X^1\Sigma^+_{0+}$ transition, which are all in the order of milliseconds. It is expected that the present theoretical study could stimulate further experimental interests on predissociation mechanisms and the properties of various excited states of the silicon monochloride cation.

Acknowledgment. This work is supported by the National Natural Science Foundation of China (Nos. 20573119, 20673127, 20733005), the Chinese Academy of Sciences and Ministry of Science and Technology. Some of the computations were carried out at the Virtual Laboratory of Computational Chemistry, Computer Network Information Center of the Chinese Academy of Sciences.

References and Notes

(1) Grill, A. *Gold Plasma in Materials Fabrication*; IEEE Press: New York, 1994; Chapter 8, p 216.
(2) Lieberman, M. A.; Lichtenberg, A. J. *Principles of Plasma Discharges and Materials Processing*; Wiley and Sons: New York, 1994; Chapter 15, p 472.
(3) Inspektor-Koren, A. *Surf. Coat. Technol.* **1987**, *33*, 31–48.
(4) Sherman, A. *Chemical Vapor Deposition for Microelectronics*; Noyes Publications: Park Ridge, NJ, 1987.
(5) Ban, V. *J. Electrochem. Soc.* **1975**, *122*, 1389–1391.
(6) Grossman, E.; Avni, R.; Grill, A. *Thin Solid Films* **1982**, *90*, 237–241.
(7) Sakai, T.; Sakai, A.; Okano, H. *Jpn. J. Appl. Phys.* **1993**, *32*, 3089–3093.
(8) Cunge, G.; Inglebert, R. L.; Joubert, O.; Vallier, L.; Sadeghi, N. *J. Vac. Sci. Technol., B* **2002**, *20*, 2137–2148.
(9) Cunge, G.; Kogelschatz, M.; Joubert, O.; Sadeghi, N. *Plasma Sources Sci. Technol.* **2005**, *14*, S42−S52.
(10) Tsuji, M.; Mizuguchi, T.; Nishimura, Y. *Can. J. Phys.* **1981**, *59*, 985–989.
(11) Weber, M. E.; Armentrout, P. B. *J. Phys. Chem.* **1989**, *93*, 1596–1604.
(12) Fisher, E. R.; Armentrout, P. B. *J. Phys. Chem.* **1991**, *95*, 4765–4772.
(13) Sumiyoshi, Y.; Tanaka, K.; Tanaka, T. *Chem. Phys. Lett.* **1993**, *214*, 17–21.
(14) Reid, C. J. *Chem. Phys.* **1996**, *210*, 501–511.
(15) Marijnissen, A.; ter Meulen, J. J. *Chem. Phys. Lett.* **1996**, *263*, 803–810.
(16) Fan, W. Y.; Liu, Z.; Davies, P. B. *J. Mol. Spectrosc.* **1998**, *191*, 98–107.
(17) Nishimura, Y.; Mizuguchi, T.; Tsuji, M.; Obara, S.; Morokuma, K. *J. Chem. Phys.* **1983**, *78*, 7260–7264.
(18) Bauschlicher, C. W., Jr.; Partridge, H. *Chem. Phys. Lett.* **1997**, *276*, 47–54.

(19) Ren, T. Q.; Ding, S. L.; Yang, C. L. *J. Mol. Struct. (THEOCHEM)* **2005**, *728*, 159–166.
(20) Šurkus, A. *Spectrochimica Acta, Part A* **2004**, *60*, 2185–2187.
(21) Woon, D. E.; Dunning, T. H., Jr *J. Chem. Phys.* **1993**, *98*, 1358–1371.
(22) Liu, K.; Bian, W. *J. Comput. Chem.* **2008**, *29*, 256–265.
(23) MOLPRO, a package of ab initio programs designed by: Werner, H.-J.; Knowles, P. J. Version 2002.6, with contributions from: Amos, R. D.; Bernhardsson, A.; Berning, A.; Celani, P.; Cooper, D. L.; Deegan, M. J. O.; Dobbyn, A. J.; Eckert, F.; Hampel, C.; Hetzer, G.; Knowles, P. J.; Korona, T.; Lindh, R.; Lloyd, A. W.; McNicholas, S. J.; Manby, F. R.; Meyer, W.; Mura, M. E.; Nicklass, A.; Palmieri. P.; Pitzer, R.; Rauhut, G.; Schütz, M.; Schumann, U.; Stoll, H.; Stone, A. J.; Tarroni, R.; Thorsteinsson, T.; Werner, H.-J.
(24) Werner, H.-J.; Knowles, P. J. *J. Chem. Phys.* **1985**, *82*, 5053–5063.
(25) Knowles, P. J.; Werner, H.-J. *Chem. Phys. Lett.* **1985**, *115*, 259–267.
(26) Werner, H.-J.; Knowles, P. J. *J. Chem. Phys.* **1988**, *89*, 5803–5814.
(27) Knowles, P. J.; Werner, H.-J. *Chem. Phys. Lett.* **1988**, *145*, 514–522.
(28) Laughoff, S. R.; Davidson, E. R. *Int. J. Quantum Chem.* **1974**, *8*, 61–72.
(29) Yang, X.; Boggs, J. E. *J. Chem. Phys.* **2005**, *123*, 184304.
(30) Ben Houria, A.; Ben Lakhdar, Z.; Hochlaf, M. *J. Chem. Phys.* **2006**, *124*, 054313.
(31) Douglas, M.; Kroll, N. M. *Ann. Phys.* **1974**, *82*, 89–155.
(32) Hess, B. A. *Phys. Rev. A* **1986**, *33*, 3742–3748.
(33) Berning, A.; Schweizer, M.; Werner, H.-J.; Knowles, P. J.; Palmieri, P. *Mol. Phys.* **2000**, *98*, 1823–1833.
(34) Le Roy, R. J. LEVEL7.7: A computer program for solving the radial Schrödinger equation for bound and quasibound levels; University of Waterloo: Chemical Physics Research Report CP-661, 2005.
(35) Basis sets were obtained from the Extensible Computational Chemistry Environment Basis Set Database, version 02/02/06, as developed and distributed by the Molecular Science Computing Facility, Environmental and Molecular Sciences Laboratory, which is part of the Pacific Northwest Laboratory, P.O. Box 999, Richland, WA 99352, and funded by the U.S. Department of Energy. The Pacific Northwest Laboratory is a multiprogram laboratory operated by Battelle Memorial Institute for the U.S. Department of Energy under Contract No. DE-AC06-76RLO 1830. Contact Karen Schuchardt for further information.
(36) Bredohl, H.; Breton, J.; Dubois, I.; Esteva, J. M.; Macau-Hercot, D.; Remy, F. *J. Mol. Spectrosc.* **1999**, *197*, 28–31.
(37) Korolkov, M. V.; Weitzel, K.-M. *J. Chem. Theory Comput.* **2006**, *2*, 1492–1498.
(38) Moore, C. E. *Atomic Energy Levels*; National Bureau of Standard: Washington, DC, 1971.
(39) Okabe, H. *Photochemistry of Small Molecules*; Wiley-Interscience: New York, 1978.
(40) Heaven, M. C. *Chem. Soc. Rev.* **1986**, *15*, 405–448.

JP809618Y